JOURNAL OF CATALYSIS 151, 420–430 (1995)

Modification of the Surface Properties of Natural Phyllosilicate Sepiolite by Secondary Isomorphic Substitution

Jean-Baptiste d'Espinose de la Caillerie,[1] Vladimir Gruver, and José J. Fripiat

Department of Chemistry and Laboratory for Surface Studies, University of Wisconsin–Milwaukee, P. O. Box 413, Milwaukee, Wisconsin 53201

Received January 21, 1994; revised July 20, 1994

The alumination of sepiolite led to a material with a moderate Lewis acidity, a high surface area, a microporous character, and a cation exchange capacity (CEC). The CEC increased to 45 meq/100 g and extraframework aluminum was formed. Alumination was accompanied by an increase in the sodium content of the sample and an improvement of the thermal stability, reflected in a microporosity more stable at 400°C than in the starting material. The CEC resulting from alumination allowed for the dispersion of vanadyl cations without loss of crystallinity. Electron paramagnetic resonance spectra indicated an isolated, immobile octahedral environment compatible with charge balancing vanadyl cations and/or vanadyl species at the edges of the octahedral ribbons in the framework. Upon alumination, the activity for ethanol dehydration was increased threefold at 400°C to 85% with a selectivity for ethylene of 50%. Upon dispersion of vanadyl cations, the reactivity for ethanol conversion was further increased. The possibility to apply successfully secondary isomorphic substitution techniques to natural minerals was clearly established and it was shown to alter their surface properties considerably, as shown here on sepiolite from both spectroscopic and reactivity studies.

INTRODUCTION

Tridimensional porous aluminosilicates belonging to the family of tectosilicates, or zeolites, have been used by industry as molecular sieves and catalysts with considerable success and a very comprehensive picture of the zeolite scene has been recently published (*1*). However, being synthetic material, they are costly to produce. This limitation could be overcome by the use of abundant natural minerals: hydrous layered silicates or clay minerals. The underlying goal of our work is therefore to investigate the modification of the surface properties of clays to palliate their deficiencies, and hence create novel catalysts or catalyst supports. We recently demonstrated the possibility of lowering the charge of vermiculite by lowering its tetrahedral Al/Si ratio (*2*) and we have reported on the synthesis of a new acidic molecular sieve with a cation exchange capacity by secondary modification of natural sepiolite (*3*). Here we demonstrate its usefulness as a catalyst support (*4*).

The inherent bidimensionality of clays prevents the development of a tridimensional pore structure. However, some clay minerals such as sepiolite and palygorskite are not true phyllosilicates and have a permanent microporosity. Unfortunately, their thermal stability is poor and their acidity limited.

The structure of sepiolite is derived from talc T–O–T ribbons, expanding along the z direction with a width of three pyroxen chains along the y direction. The ribbons are linked by an inverted Si–O–Si bond. They form a staggered talc sheet with a discontinuous octahedral layer allowing for infinite channels along z (*5*). The size and geometry of the ribbons fix the width and height of the channels, 1.06×0.37 nm^2, while they extend without limitation along the length of the crystal fibers. Under natural conditions, they are filled with zeolitic water loosely H-bound to the basal oxygen planes. After outgasing at temperature $\leq$ 150°C, the total surface area is $\sim$300 m^2 g^{-1}, of which about 50% are in the zeolitic micropores with Kelvin radius $\approx$ 0.5 nm, whereas the other 50% are in the irregular inter- and intrafiber mesopores with radii $>$ 1.7 nm (*6*). Upon heating at 150°C under vacuum, half of the structural water is removed, and, as the structure folds and the micropores close (*7, 8*), the surface decreases to about 140 m^2/g. At about 450°C, the second coordination water is lost, and the edge octahedral Mg completes its coordination with the two closest oxygen of the silica surface. The folding is then irreversible.

Because the framework of the sepiolite is ideally neutral, the zeolitic water in the channels does not show acidic properties, in contrast with water coordinated with exhangeable cations in charged layer silicates. The structural water coordinated to the edge of the octahedral rib-

[1] Present address: Ecole Supérieure de Physique et de Chimie Industrielles, Laboratoire de Physique Quantique, URA 1428 CNRS, 10, rue Vauquelin, F-75231 Paris Cedex 05, France.

0021-9517/95 $6.00

bons is not acidic either, and natural sepiolite presents a basic surface with a limited catalytic activity (*9–13*), which may be attributed to smectite impurities. Furthermore, because it has no cation exchange capacity (CEC), the application of natural sepiolite as a catalyst support is limited to impregnation or precipitation techniques leading to poorly defined samples, although its low cost has prompted numerous investigations into its use as a catalyst support for impregnation or deposition of Mn, V, Pd, Pt, and Ni (*14–18*).

Depite all the activity in the field of zeolite secondary modification, modifications of clays have been limited to cation exchanges (*19*), pillaring (*20*), or octahedral substitutions. For example, it has been known since the sixties that in sepiolite treated by 6 *M* NaOH at 95°C the exchange of the edge octahedral sites is large (*21*). Sepiolite treated in this way is transformed into loughlinite, which has an identical structure, but contains ~6 Mg and 4 Na instead of 8 Mg per 12 Si (*22*). Corma *et al.* realized that it is then possible to exchange the edge Na with any other monovalent, divalent, or trivalent cations of smaller ionic radius by simple cation exchange techniques in a polar medium (*23*). They were able to exchange between 50 and 170 meq/100 g of the octahedral cations, and based their claim to the exchange on XRD data. They applied this technique to the preparation of Cu^{2+} (*24*), K^+ (*25*), Li^+, Cs^+ (*26*), Al^{3+}, Cr^{3+}, and H^+ (by leaching with 1 *M* HCl) (*27*) sepiolites. They observed a slightly improved thermal and hydrothermal stability for the K and Al derivatives. Pyridine adsorption reveals a considerable increase in the number of Lewis acid sites on the Al–sepiolite *versus* the original sepiolite, as well as Brønsted sites, apparent up to a desorption temperature of 150°C (*28*). Their work is the only report of a sepiolite or a modified sepiolite showing Brønsted acidity by pyridine adsorption. Those sites are strong enough for skeletal isomerization and cracking of methylcyclohexene at 350°C. Al–sepiolite so prepared is quite active for the dehydration of ethanol into ethylene and diethyl ether, with a product distribution similar to those obtained for silica–alumina and zeolites (*29*). The origin of the Brønsted acidity is in the highly polarized water molecule bonded to the Al at the edges of the octahedral ribbons. Mg and Na sepiolites have no Brønsted acidity because the charge to radius ratio of these cations is low and so is their polarizing power.

An important advance for the possible use of sepiolite in catalysis would be to exchange some Si in the tetrahedral layer by Al. This would result in a net lattice negative charge making possible transition metal cation exchange procedures provided that the specific surface area remains in the range of those reported for unmodified sepiolite. Our work has shown that such tetrahedral substitutions are possible (*3*). Alumination of sepiolite could be achieved by treating the mineral with a solution of sodium aluminate and sodium hydroxide. Both tetrahedral and octahedral aluminum were introduced into the structure, while some silicon and magnesium were leached out. The net negative charge of the lattice increased by a factor of ~3, consequently, the aluminated sepiolite became a cation exchange. A small amount of nonframework alumina species was dispersed within the porous system. While in the initial material irreversible folding occurs below 400°C under vacuum, it was delayed to higher temperature in the aluminated mineral. The acidity of the aluminated sepiolite was mainly of the Lewis type, although Brønsted sites must also exist. Bifunctional catalysts could be produced by taking advantage of their cation exchange capacity. However, the reproducibility of the alumination procedure was poor. Catalytic studies require better defined samples. We therefore turned our attention to an alumination method where the reaction parameters are more controlled, hoping for better reproducibility. This was achieved under mild hydrothermal conditions. The characterization and reactivity performance of this new set of samples are described here. We present an in-depth characterization of a sample prepared under optimized conditions leading to the isomorphic substitutions of more than 20% of the original silicon while maintaining the structural integrity of the sepiolite. A brief reactivity test of the potential of this new material as catalyst and catalyst support is also presented here, and a detailed catalytic study will be published in a subsequent paper (*30*).

EXPERIMENTAL

Synthesis

Materials. The original sepiolite was provided by Tolsa S.A. (Spain). It is commercialized under the trade name Pangel-S (*31*). Pangel-S is very low in aluminum and iron, thus its CEC is small, 5 meq/100 g. All other reagents are ACS reagent grades obtained through commercial suppliers.

Alumination procedure. Pressurized reactions were performed in a 300-cm^3 bomb reactor equipped with a stirring axis, a heating mantle, and a thermocouple (Parr 4561 mini reactor). The temperature was controlled to within less than a degree (Parr 4841 controller). In the Teflon liner, 3 g of sepiolite was suspended in 150 cm^3 of 0.115 *M* $NaAlO_2$, 6 *M* NaOH aqueous solution. The reactor was sealed and the temperature allowed to rise to 120°C in 20 min. The temperature was maintained at this level for a total reaction time of 5 h (including the heating ramp). Before opening, the bomb was left to cool outside the heating mantle until the temperature dropped

to 80°C. The whole operation was performed under continuous stirring (270 rpm).

Washing. The solids were separated from the solutions by centrifugation and carefully washed with diluted NaOH and NH_4OH aqueous solutions following a published procedure (*3*).

Cation exchanges. By the end of the synthesis and washing, the exchangeable cation was NH_4^+. Some samples were further exchanged with $VO(H_2O)_5^{2+}$, readily available from the dissociation of $VOSO_4$ in water (*32*). The color is blue. It is easily oxidized to V(V) in basic solution, and the concentration must be kept under 0.05 *M* in order to operate the exchange at pH > 3. Consequently, the aluminated sepiolite was added to a 0.02 *M* $VOSO_4$, 50/50 v/v, mixture of water and ethanol (100 w/w liquid/solid). The initial pH of the solution was 3.4 and it increased to 3.9 upon addition of the solid. After overnight stirring at room temperature in a closed Erlenmeyer flask, the suspension was centrifuged. The final pH of the solution was 3.4 and its color was blue. The solid was washed eight times with 25 cm^3 of water acidified to pH = 3 with H_2SO_4. It was then rinsed with distilled water five times. The variation in pH as well as the slightly greenish color of the sample suggested that despite the low concentration, the high liquid/solid ratio, and the presence of ethanol, some vanadyl had been hydrolyzed. However, no change of color to orange indicative of oxidation occurred.

Characterization

Cation exchange capacity. Since by the end of the synthesis the samples were in their ammonium form, the CEC could be obtained by a simplified Kjeldahl digestion of nitrogen (*33*).

Chemical analysis. Chemical analyses were performed on samples calcined at 900°C and fused at 1050°C.

Magic angle spinning nuclear magnetic resonance. The magic angle spinning nuclear magnetic resonance (MAS–NMR) one-pulse experiments were performed on a GN-500 spectrometer with pulse length corresponding to a flip angle of *circa* 10° at which value only the central transition is excited, therefore avoiding deformation of the lines (*34*). The parameters were as follows. For ^{27}Al: rf 130.3 MHz, pulse 0.5 μs, delay of 50 ms. The chemical shifts were referred to a 0.1 *M* $AlCl_3$ aqueous solution. For ^{51}V: rf 131.5 MHz, pulse 1 μs, delay 50 ms. The reference was a 0.03 *M* VO_3^- solution obtained by dissolving the appropriate amount of NH_4VO_3 in a NaOH solution and then adjusting the pH to 10. This solution was used as a secondary reference at −527 ppm relatively to $VOCl_3$. More details can be found elsewhere (*3, 35*).

Nitrogen adsorption. Prior to adsorption, the samples were pretreated under vacuum at further specified activation temperatures. Complete full-sorption isotherms were performed at 77 K with an automated gas sorption analyzer (Coulter Omnisorb 100) in the static mode. The adsorption isotherms were interpreted in terms of the BET method (surface areas), the *t*-plot method (micropores and external surface areas), and the BJH method assuming a cylindrical pore shape (macropores) (*36*).

FTIR and pyridine sorption. Self-supported films (2–4 mg/cm^2) were prepared through the evaporation of an aqueous suspension on a sheet of Mylar. They were mounted on a glass holder in a greaseless, high-vacuum cell fitted with an oven for outgassing the sample at controlled temperature. The pyridine was kept on KOH prior to use and on dry zeolites during the experiments. It was thoroughly dried before each sorption by several cycles of evacuations while frozen at liquid nitrogen temperature. The samples were exposed to about 30 Torr of pyridine for 10 min and degassed at controlled temperature for 20 min. The spectra were recorded with a Nicolet FTIR instrument. Its maximal resolution is 2 cm^{-1}. 600 accumulations were performed for each spectrum.

Electron paramagnetic resonance. Electron paramagnetic resonance (EPR) measurements were performed on a Varian E-115 spectrometer (X band, 9.1 GHz of microwave frequency with a field strength of about 3500 G) at room temperature. A field modulation of 100 kHz was used with a modulation amplitude of 2 G. The *g* values were referred to a DPPH standard. The range of 2000 G was scanned in 8 min.

Reactivity tests. Reactivity tests were performed in a conventional, home-built, atmospheric pressure, greaseless, laboratory flow system with He as a carrier gas. Except for the glass reactor, the system was made of $\frac{1}{4}$" stainless steel tubes. The whole system was confirmed to be inert for ethanol conversion at our operating temperatures by experiments without catalysts in the reactor. The reactants were fed through a motor-driven gas-tight syringe to the heated mixing chamber where it vaporized. Between 0.1 and 0.25 g of sample sat in the fixed-bed, thermostated, tubular reactor. The samples were activated overnight *in situ* under a He stream of 5 liters/h at reaction temperatures. Product analysis was performed on line by conventional gas chromatography. The GC was a Gow-Mac 69-350 chromatograph fitted with a column 23% SP-1700 on 80/100 Chromosorb PAW. Diffusion control was tested by varying the flow rate and the mass of catalyst at fixed contact time. Note that measurements were not performed at low conversion regime and therefore no information on rates was obtained. Results are reported in C atom units.

RESULTS

Structural Characterization of Aluminated Sepiolite

The samples prepared under mild hydrothermal conditions, 120°C in a sealed vessel, yielded higher CEC (45 meq/100 g) than previously published results (*3*).

Crystallinity. The XRD of the sample aluminated in a sealed vessel was similar to the pattern of the original sepiolite (Figs. 1a and 1b), except for a loss of crystallinity reflected in the decreased intensities of the peaks. No other crystalline phases were apparent. The thermal stability of the 12 Å line was better than in the samples prepared with an open batch (*3*) as it remained well defined at 450°C (Fig. 1d). A weak reflection at 10 Å characteristic of the folded sepiolite was nevertheless observed concurrently, indicating that the folding did not occur homogeneously in all the crystals, but that some domains folded before others. If the increased thermal stability was due to the alumination, this could be an indication that the alumination was not homogeneous across all the crystallites.

Textural properties. The loss of crystallinity observed by XRD was also reflected in a loss of total surface area and micropore volume (Fig. 2). The mesopore volume (*circa* 0.5 cm^3/g) and the external surface area (*circa* 150 m^2/g) were not affected by alumination. The sharp loss in surface area and micropore volume experienced by the natural sepiolite upon folding under vacuum between 150 and 200°C was not observed in the aluminated sample. Instead, the loss of surface area and microporosity was gradual between 200 and 400°C. At 400°C, the sample retained a micropore volume equivalent to 20% of that of the unfolded natural sepiolite. This suggested, in agreement with the XRD data, that the structure was not entirely folded at this temperature. Except for a small sintering effect, the mesopore volume was not affected by thermal treatment in the natural sepiolite or in the aluminated sample.

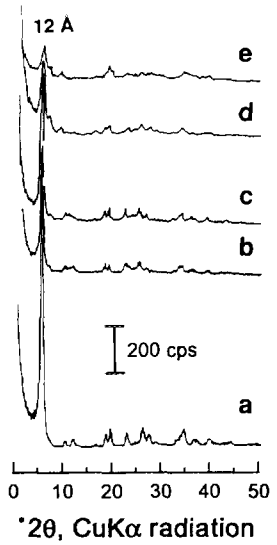

FIG. 1. XRD powder spectra of (a) ammonium-exchanged natural sepiolite, (b) ammonium-exchanged aluminated sepiolite, (c) vanadyl-exchanged aluminated sepiolite, (d) ammonium-exchanged aluminated sepiolite treated at 450°C, and (e) vanadyl-exchanged aluminated sepiolite treated at 450°C.

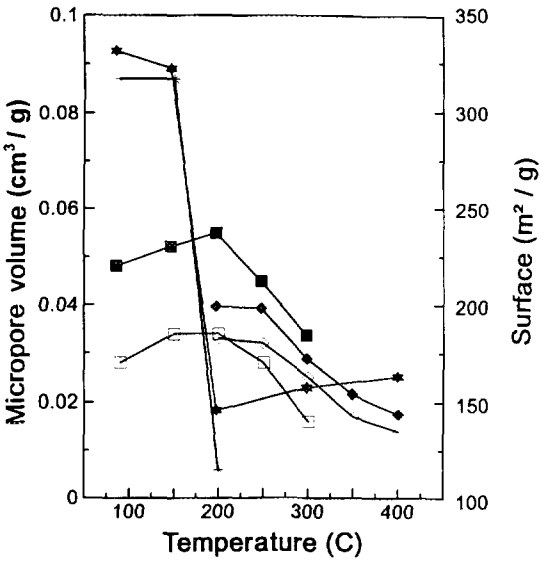

FIG. 2. Nitrogen adsorption results (total surface and micropore volume) after thermal activation under vacuum of ammonium-exchanged natural sepiolite (★, BET; *, *t*-plot), ammonium-exchanged aluminated sepiolite (■, BET; □, *t*-plot), and vanadyl-exchanged aluminated sepiolite (◆, BET; ◇, *t*-plot).

Chemical analysis. Knowing the approximate mass of the unit cell of sepiolite, it is possible to calculate its composition from the chemical analysis assuming the stoichiometry of the oxides (Table 1):

$$M^{+}_{0.51}(Si_{11.79}Al_{0.2})^{IV}(Mg_{7.17}Al_{0.3}Fe^{3+}_{0.10}Ti_{0.01})^{VI} O_{30}(OH)_4(OH_2)_4.$$

The Al content was low, and the CEC was calculated to be 4 meq/100 g, very close to the measured value of 5 meq/100 g. The same calculations for the aluminated sample led to an excess of Al. It was therefore necessary to assume the occurrence of an extraframework species. This should lead to an uncertainty on the mass of the unit cell, or, alternatively if the mass is fixed, on the theoretical number of oxygen per unit cell mass. However, because the deviation from the predicted number of 32 oxygens assuming the stoichiometry of the oxides was small

TABLE 1

Chemical Analyses of Calcined (900°C) Samples

	NH_4-Pangel-S (g)	NH_4-aluminated sepiolite (g)	VO-aluminated sepiolite (g)
SiO_2	58	52	48
Al_2O_3	2.1	17.8	16.2
TiO_2	0.09	0.09	0.1
Fe_2O_3	0.68	0.54	0.5
MgO	23.67	26.9	25.9
CaO	0.55	0.19	0.1
Na_2O	0.1	1.15	—
K_2O	0.53	0.37	—
V	N/A	N/A	4.61
Total	85.72	96.79	95.41
CEC (meq/100 g)	5	45	N/A

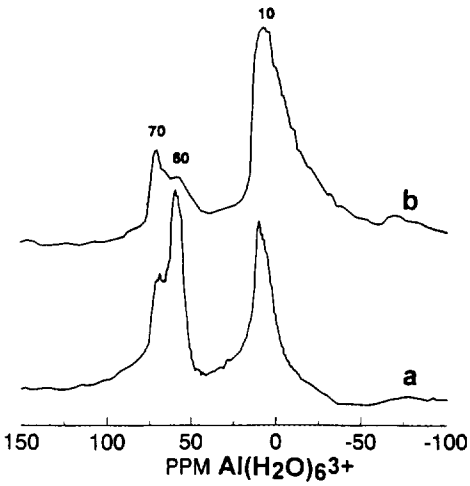

FIG. 3. ^{27}Al MAS–NMR of (a) aluminated sepiolite and (b) vanadyl-exchanged aluminated sepiolite. Spinning at 10 kHz.

(32.2), we set the scaling factor to unity and obtained the following structural formula:

$$M^{+}_{1.85}(Si_{9.33}Al_{2.67})^{IV}(Mg_{7.19}Al_{0.72}Fe^{3+}_{0.071}Ti_{0.01})^{VI} O_{30}(OH)_4(OH_2)_4 \cdot (Al_{0.37})^{NF}$$

It was remarkable that if all the nonframework (NF) Al species carried a nominal charge of +1, the calculated CEC matched exactly the measured value of 45 meq/100 g, leading to a fully balanced charge. Upon alumination, the $(Al)^{IV}_F$ content went from 0.2 to 2.67, and the $(Al/Si)^{IV}$ ratio was 0.29. Note that there was a non-negligible amount of nonexchangeable Na.

MAS–NMR. Except for line broadening and new weak lines attributable to Al deshielding, the ^{29}Si MAS–NMR spectrum of the aluminated sample was identical to the natural sepiolite one. Apart from being an indication that the sepiolite structure was maintained upon alumination, the interpretation of the sepiolite and aluminated sepiolite spectrum is not crucial to this study and is presented elsewhere (*35*). The case for isomorphic substitutions was made by ^{27}Al MAS–NMR (Fig. 3a). The ^{27}Al MAS–NMR spectra revealed clearly that alumination occurred. In the starting material, as there is only a very small amount of aluminum, the intensity of the ^{27}Al signal was negligible. In the aluminated sepiolite, the ^{27}Al MAS spectra contained three resolved contributions at 70 ± 1 ppm, 60 ± 2 ppm, and 9 ± 1 ppm. The first two are assigned to Al^{IV}, respectively at the center and at the edge of the structural ribbons, and the last one to Al^{VI}, both substituted in the octahedral layer by removal of the edge Mg and outside of the framework. This assignment has been discussed previously when describing alumination of sepiolite by an open batch technique (*3*). The major contribution was the tetrahedral line at 60 ppm, and there was apparently more $(Al)^{IV}$ than $(Al)^{VI}$. The relative intensities of the $(Al)^{IV}$ and $(Al)^{VI}$ lines matched well with that which was calculated from chemical analysis.

Acidity measurements. In line with Parry's work (*37*) on the adsorption of pyridine on alumina, the FTIR spectrum of pyridine adsorbed on aluminated sepiolite led to the observation of the bands characteristic of coordinatively bound pyridine (1450 cm^{-1}) while no pyridinium ions (1540 cm^{-1}) were detected: only Lewis acidity, and none of the Brønsted type, was shown (*37*), regardless of the pretreatment temperatures investigated, namely 200°C and above. The integrated intensity of the 1450 cm^{-1} peak led to a relative estimate of the amount of Lewis sites retaining coordinatively bound pyridine at a given desorption temperature (Fig. 4). It must be noted that the mean steric hindrance for pyridine is 0.59 nm, which does not compare favorably with the Kelvin radius of the micropores (≈ 0.5 nm). Therefore only strong Brønsted acid sites could provide a sufficient driving force for the diffusion of pyridine within the zeolitic channels at room temperature. Apparently, they are no such sites in the aluminated sepiolite.

Vanadium Dispersion

The cation exchange capacity of the aluminated sepiolite provided a driving force for the diffusion and the retention of the vanadyl cations within the pores. The V loading after exchange was 0.10 atom/100 g. It is impossible to assume the stoichiometry of the V exchange of the aluminated sample and to suggest a structural formula without knowing the oxidation state of the V species. Note that Na was removed during the VO^{2+} exchange.

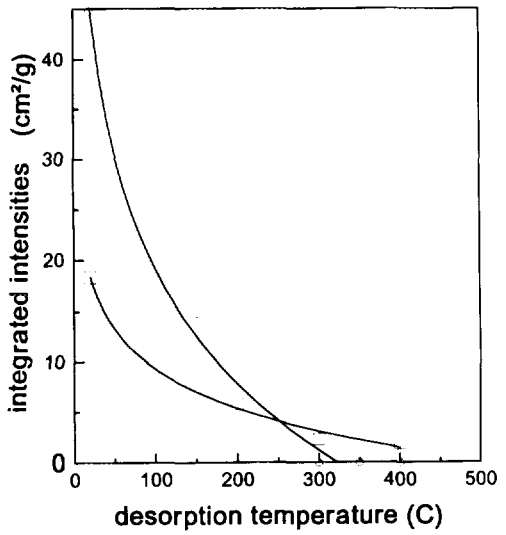

FIG. 4. Amount of coordinatively bound (Lewis acidity) pyridine estimated from the 1450 cm^{-1} FTIR band on aluminated sepiolite exchanged with (○), NH_4^+ or (□) VO^{2+} and pretreated at 400°C versus desorption temperature. Framework background is subtracted.

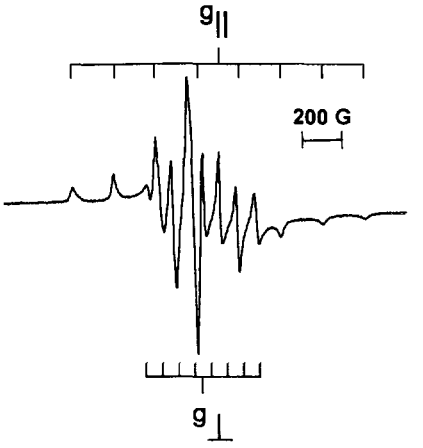

FIG. 5. EPR spectrum at room temperature of vanadyl-exchanged aluminated sepiolite.

The XRD spectrum after V exchange was identical to the spectrum of the aluminated sample (Fig. 1c). No extra-framework crystalline vanadium species was detected. On the other hand, the absence of significant displacement of the peak positions indicated that the unit-cell dimensions were not altered by the exchange. Both facts showed that for the most part only cation exchange took place. This was confirmed by the similar surface areas and pore volumes (Fig. 2) of the aluminated sample before and after V exchange.

In order to elucidate the nature of the V species, we reverted to spectroscopic techniques. Unfortunately, it was not possible to detect by FTIR the V=O stretching vibration because of the overlap with Si–O lattice vibrations (*38*).

EPR. The EPR spectrum of the vanadyl-exchanged sample exhibited two sets of eight lines (Fig. 5). The hyperfine splitting in eight lines was characteristic of the interaction of an electron with the nuclear magnetic moment of the 7/2 spin nuclei of ^{51}V (natural abundance 99%). It reflected an unpaired electron density on the vanadium ion and was attributable to a V(IV) species, namely VO^{2+}. The two sets of lines reflected the anisotropy and the axial symmetry of the ligand field of the vanadium complex in the magnetic field. It was typical of a V(IV) complex with square pyramidal coordination, that is, a nearly octahedral site with a tetragonal distortion. The ligand along the z axis ($g_\parallel$) is the oxygen from the V=O bond of VO^{2+}. The other oxygens are similar enough for an axial geometry of the vanadium complex ($g_x \equiv g_y \equiv g_\perp$). The high ratio $A_\parallel/A_\perp$ reflected the fact that the axial component (V=O) was the most covalent, while the high value of $g_\parallel/g_\perp$ indicated a strong tetragonal distortion of the field symmetry. The values of the g tensor agreed with those reported for octahedrally coordinated (square bipyramid D_{4h} ligand symmetry) vanadyl in zeolitic channels (*39*). The fact that this anisotropy was not averaged by motion indicated that the V(IV) species was restricted, either by the limited size of the channels, precipitation of a hydrolysis product, or interaction with the sepiolite framework. Indeed, the overall shape of the spectrum and the magnetic parameters (Table 2) are strikingly similar to those obtained for VO^{2+} immobilized within zeolites, either by cooling at 77 K or at room temperature by interaction with the framework (*40, 41*). On the contrary, the values of the hyperfine splitting constants for $VO(H_2O)_5^{2+}$ immobilized at liquid N_2 temperature between hydrated hectorite layers reported by McBride (*42*) are significantly different. This is not surprising, as if the vanadyl was located in the micropores, as the comparison with VO^{2+} in zeolitic cavities would suggest, the height of the sepiolite channels (0.37 nm) would not accommodate a two-layer hydrate (≈ 0.45–0.50 nm).

TABLE 2

EPR Magnetic Parameters

Sample	T (K)	$g_\parallel$	$g_\perp$	$A_\parallel$ (G)	$A_\perp$ (G)	Ref.
VO-aluminated sepiolite	RT	1.939	1.984	193 ± 3	74 ± 1	this work
$VO(H_2O)_5^{2+}$	77	1.933	1.976	201 ± 1	75.5	(41)
VO–Y	77	1.938	1.983	197 ± 1	75	(40)
VO–hectorite	77			204	81	(42)

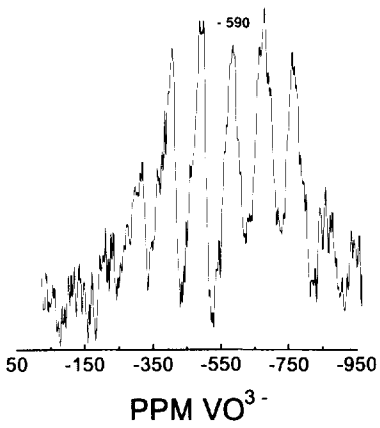

FIG. 6. ^{51}V MAS–NMR of vanadyl-exchanged aluminated sepiolite. Spinning at 10.5 kHz.

MAS–NMR. The ^{27}Al spectrum was significantly broadened by interaction with the paramagnetic V(IV) species (Fig. 3b). The $(Al)^{IV}$, and especially the 60 ppm contribution, was particularly suppressed by the broadening and screening of the magnetic field by VO^{2+}. Indeed this paramagnetic cation was likely to be close to the $(Al)^{IV}$ responsible for the charge deficit of the structure. Because NMR cannot probe paramagnetic species, the ^{51}V NMR signal demonstrated that part of the vanadyl cations was oxidized to V(V). Probably because V(V) was much less abundant than the paramagnetic V(IV), a static NMR signal was not observable, even after 30,000 accumulations. Under MAS performed at varying speeds a ^{51}V MAS–NMR signal was collected after 23,000 accumulations (Fig. 6). The spectra were complicated by the intense spinning side-band pattern due to the abundance of paramagnetic V(IV), reflecting on both a large chemical shift tensor and quadrupole satellite interactions (*43*). However, at least one contribution with a maximum at -590 ± 5 ppm from VO_3^- was detected by varying the spinning rate. The second-order quadrupolar shift has been determined to be small at 11.7 *T* in model compounds (*44*) as well as in supported species (*45*). Consequently, the maximum detected at high speed reflects the isotropic chemical shift without second-order quadrupolar correction.

Surface acidity. The aluminated sepiolite had fewer acid sites after exchange with transition metal cations (Fig. 4). The V sample was able to retain some pyridine, even at 400°C. The decreased number of acid sites can be related to the saturation of the sites by near-lying vanadyl groups. The stronger Lewis acid sites present in the vanadyl-exchanged sample were related to unsaturated V sites generated upon dehydration before pyridine adsorption. Tetrahedral V(V) species resulting from the dehydration of pentacoordinated species are known to occur on silica-supported vanadium oxide (*46*). These V sites could be tentatively assigned to those stronger Lewis sites absent in the original aluminated sepiolite, following the suggestion of Centi *et al.* on V–silicalite (*39*).

Reactivity Test

Ethanol is not presently an economical feed for the production of olefins; however, alcohol conversion proceeds *via* dehydration and dehydrogenation, therefore probing both acid/base and redox functions. As we wanted to investigate the surface properties of the modified sepiolite, ethanol conversion seemed particularly appropriate, especially considering the wealth of literature on ethanol conversion on zeolites (*47*). With its cross-section area of 0.23 nm^2, ethanol is able to enter the structural micropores and probes all the surface area thereby showing up the catalytic properties of sepiolite.

The conversion of ethanol was performed at 280 and 400°C with a partial pressure in the feed of 25 Torr. The contact time ranged from 4 to 30 min g mol^{-1} at 400°C and from 0.25 to 200 h g mol^{-1} at 280°C.

At 400°C, the evolution of the products with the time on stream for the vanadium sample showed a very brutal deactivation in the first minutes of reaction. The deactivation followed a biexponential that could be rationalized by two regimes of deactivation by coke (the samples contained up to 26% w/w C after reaction): first a very fast closure of the residual micropores, then a slower coverage of the mesopore surface. It is therefore important to distinguish between the initial and the subsequent conversions. Results obtained at 400°C with a contact time of 17 min g mol^{-1} (the contact time was found not to affect significantly the selectivity within the range studied) are presented in Table 3. Initially, the natural sepiolite dehydrated ethanol (~25%) with a higher selectivity for ether (65%) than for ethylene (35%). The amount of butadiene produced was insignificant. Upon alumination, the added acidity increased the activity by at least threefold to reach a total conversion of almost 85% with an equal amount of ether and ethylene produced, while small amounts of butadiene were detected (2% selectivity). On the V-exchanged aluminated sepiolite, substantial amounts of acetaldehyde (12%) and butadiene (6%) were produced.

Working at 280°C presents two advantages: the microporosity is fully opened at this temperature, and the coke formation is considerably less than at higher temperature. The catalytic activity still dropped steeply in the initial stage, but it levelled off afterward and remained constant within 10% for more than two days on stream. During this period of constant activity, the selectivity is independent of total conversion. The major products on vanadyl-exchanged aluminated sepiolite were ether

TABLE 3

Ethanol Conversion at 400°C with Contact Time 17 min g mol^{-1} and 25 Torr Ethanol Feed

Sample	Time on stream	Conversion (%)	Selectivities				
			Ethylene	Ether	Butadiene	Acetaldehyde	Other C_4
Pangel-S	2 min	25	35	65			
	10 h	10	30	70			
Aluminated sepiolite	2 min	85	48	50	2		
	10 h	42	29	71			
VO-aluminated sepiolite	2 min	100	65	10	6	12	6
	10 h	20	52	29		19	

(65%) and ethylene (24%), while the minor products were acetaldehyde (8%), butadiene (2%), and butenes (1%) (Fig. 7). A general reaction scheme for ethanol conversion is shown in Fig. 8.

When we added a large excess of acetaldehyde to the ethanol, we observed an increase of the yield of butadiene (Fig. 9) with a very high selectivity (about 80%), and this regardless of the presence of vanadium on the catalyst (Fig. 10). All other product yields fell below 2% and could not be accurately quantified.

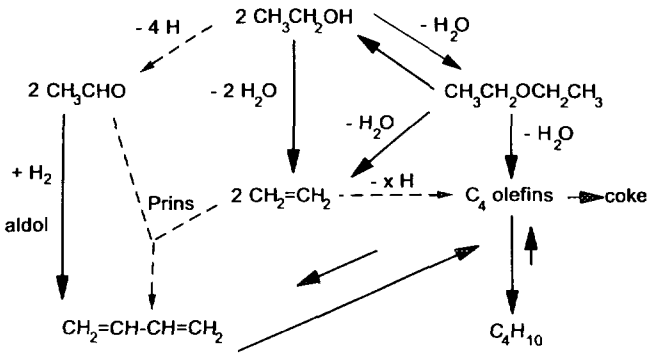

FIG. 8. General reaction scheme for ethanol conversion on our bifunctional catalyst showing putative routes to observed products.

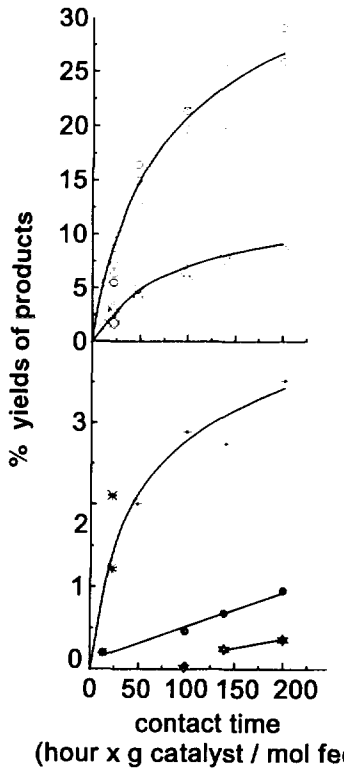

FIG. 7. Conversion of ethanol on V-exchanged, Al-modified sepiolite as a function of contact time at 280°C and with 25 Torr of ethanol in He: (○) diethyl ether, (◇) ethylene, (*) acetaldehyde, (●) butadiene, and (★) butenes.

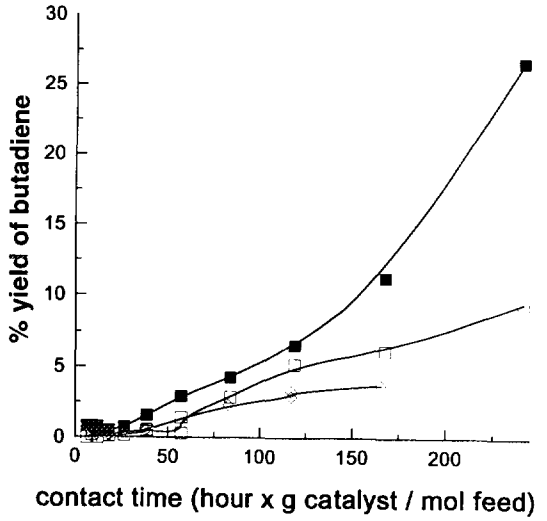

FIG. 9. Yield of butadiene from ethanol with an excess of acetaldehyde on aluminated sepiolite at 280°C: (■) without vanadium, 25 Torr ethanol, and 25 Torr acetaldehyde; (□) with vanadium, 25 Torr ethanol, and 25 Torr acetaldehyde; (◇) with vanadium, 6 Torr ethanol, and 25 Torr acetaldehyde.

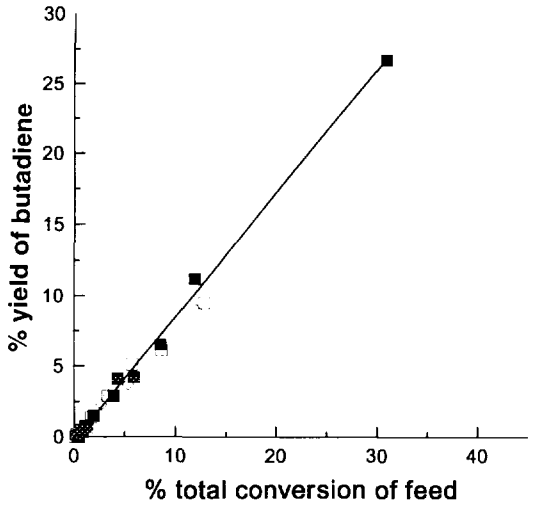

FIG. 10. Selectivity for butadiene from ethanol with an excess of acetaldehyde on aluminated sepiolite at 280°C: (■) without vanadium, 25 Torr ethanol, and 25 Torr acetaldehyde; (□) with vanadium, 25 Torr ethanol, and 25 Torr acetaldehyde; (◇) with vanadium, 6 Torr ethanol, and 25 Torr acetaldehyde.

DISCUSSION

The chemical and oxidation state of the vanadium on the aluminated sepiolite is particularly important as it is likely to affect the catalytic activity. For example, vanadium exchanged, impregnated, or isomorphically substituted onto zeolites exhibits very different catalytic behavior toward selective oxidation (*48*) and ammoxidation (*49*). The resolution of the EPR hyperfine splitting showed that the spin–spin dipolar interaction broadening was minimal and that the paramagnetic centers were far apart. The EPR data clearly revealed the occurrence of an immobile monomeric V(IV) species in octahedral coordination. This species was located within the zeolitic channels as indicated by its restricted mobility and by its relation of proximity with the aluminum framework apparent in the poisoning of some of the Lewis acidity upon vanadyl exchange as well as in the selective suppression of the framework $(Al)^{IV}$ ^{27}Al MAS–NMR signal at 60 ppm by paramagnetic screening. A close association between extralattice paramagnetic V(IV) and structural spin 5/2 aluminum has been detected by spin–echo in V–ZSM-5 (*50*). As already pointed out, Martini *et al.* (*40*) obtained EPR magnetic parameters extremely close to ours for vanadyl-exchanged zeolite Y, from which they were able to extract bond coefficients. Their results indicate an increase in the covalent character relative to free $VO(H_2O)_6^{2+}$ of the four in-plane bonds. It is conceivable that, since the height of the zeolitic channel does not accommodate a two-layer hydrate, some of the ligand sites in the octahedral coordination shell of V(IV) were occupied by basal lattice oxygens or structural water. Isolated partially hydrated vanadyl cations in octahedral coordination were positioned in the channels and in the pores, accessible to any molecule entering them. In other words, the dispersion of the vanadyl cations was good. This characteristic is very different from what could be expected for impregnated samples, the only possible dispersion method on neutral natural sepiolite. This latter fact is of catalytic significance as it is well established that the activity toward the oxidation of alcohols is related to the number of surface vanadyl ions dispersed on alumina (*51*) as well as on silica (*52*).

The ^{51}V NMR signal revealed that part of the vanadium had been oxidized to V(V) but this was a minor occurrence as shown by the strong SSB pattern in MAS, the absence of a detectable static spectrum, and the very intense V(IV) EPR signal. Although not necessarily relevant to the catalysis of the present system, the question nevertheless arises as to the exact nature of the V(V) species. Unfortunately, the paramagnetic shift due to the abundant V(IV) species is likely to be important here and precludes comparison with values of chemical shifts reported for hydrated vanadium oxide species supported on oxides. A broad signal around −590 ppm corresponding to four-coordinate V(V) in amorphous magnesium vanadates was observed by Occelli *et al.* on natural sepiolite impregnated with vanadyl naphthenate after calcination at 540°C (*53*). Nevertheless, the well-resolved MAS pattern observed in this study bore no resemblance in shape to the broad line observed by Occelli *et al.* Clearly, the vanadate phase did not form at room temperature (*54*). It must be noted that due to the small number of V(V) sites, the NMR signal was not sufficiently strong and detailed to be able to distinguish between sites anchored at the basal surface of the aluminated sepiolite within the channels and substitutional octahedral sites at the edges of the ribbons as suggested to occur in V-impregnated natural sepiolite (*14*).

The modifications of the surface properties of sepiolite upon alumination were also clearly reflected by the new catalytic behavior. Alumination of the sepiolite resulted in an increased Lewis acidity detected by pyridine adsorption. This acidity was responsible for the increased dehydration activity of the aluminated sample. At least some of those sites were located outside the framework since the catalyst remained active after pore blockage by coke. In that respect, the absence of detection by FTIR of pyridinium ions is interesting considering that Al substitution results in Brønsted sites upon thermal activation of zeolite. As previously stated, this original behavior of sepiolite can be rationalized in terms of the hindered diffusion of pyridine within the channels, but it must also be noted that, contrarily to the reactivity test, the pyridine sorption experiments were performed under vacuum un-

der which conditions dehydroxylation of Brønsted sites into Lewis sites is facilitated. Consequently the fact that no pyridinium ions were detected does not imply that no Brønsted sites are available in the catalyst, but that the eventual ones would be weaker than the ones found on zeolites. The analysis of the reactivity after vanadyl exchange is more complex. Clearly, the dispersion of vanadyl cations was responsible for the acceleration of the ethanol conversion, but the path leading to butadiene was less clear. It is evident that acetaldehyde participated in the formation of butadiene. Kitayama *et al.* (*14*) observed selectivities larger than 20% for 1,3-butadiene on both Mn- and V-supported sepiolite at 280°C in a recirculation reactor where significant amounts of acetaldehyde accumulated (up to 20% of the C in the closed system). They suggested that two molecules of acetaldehyde could condense to form butadiene. This is the well-known aldol condensation in homogeneous aqueous catalysis. Because it is not known in the present study if dehydrogenation proceeds on basic or redox sites, we were not able to establish a definite reaction path and this is beyond the scope of this paper. However, the set of tests at 280°C with a mixture of ethanol and acetaldehyde provided some indications. Butadiene appeared as a secondary product of ethanol, since, at constant partial pressure of acetaldehyde, the butadiene yield increased with the partial pressure in ethanol (Fig. 9). Consequently, the reaction path did not proceed simply through an acetaldehyde condensation but at some point ethanol or one of its products was involved. Clearly, the probing of the surface activity by ethanol conversion does not substitute for a detailed catalytic study. Nevertheless, we suggest that a molecule of acetaldehyde could condense with a molecule of ethylene in a scheme similar to the so-called Prins reaction (*55*) known to occur with homogeneous catalysts in aqueous phase. The Prins reaction, also suggested by others for diene synthesis on metal/acid solid catalyst for the reaction of isobutene with isobutyraldehyde (*56*), proceeds *via* the addition of ethylene (nucleophile) to the activated carbonyl (electrophile). In other words, the ethylene acts as the hydrogen source and no H_2 is involved (there is no hydrogen transfer step).

To sum up on the reactivity probing of the surface, the dispersion of vanadium by vanadyl cation exchange on acidic aluminated sepiolite led to a bifunctional catalytic system. The presence of acid sites as well as the monodisperse vanadyl species increased the butadiene yield, although it is not clear if this happened through an acceleration of an aldol condensation scheme, as suggested on V_2O_5 impregnated natural sepiolite, or through the opening of a new route for butadiene production *via* a Prins mechanism.

CONCLUSION

Sepiolite alumination gives a material with a moderate acidity, a microporous character, and a cation exchange capacity. Extraframework aluminum was formed. Alumination occurred in tetrahedral as well as in octahedral positions in the structure. It was accompanied by an increase in the sodium content of the sample and an improvement of the thermal stability, reflected in a microporosity more stable at 400°C than in the starting material. The tetrahedral substitutions did not result in Brønsted sites strong enough to be detected by pyridine sorption as observed in calcined ammonium-exchanged zeolites, but instead in mainly a Lewis acidity. Extraframework aluminum probably also contributed to the Lewis acidity. The cation exchange capacity resulting from alumination allowed for the dispersion of vanadyl cations without loss of crystallinity. The nature of the vanadium species was not fully elucidated, but EPR evidence indicated an octahedral environment compatible with charge balancing vanadyl cations and/or vanadyl species at the edges of the octahedral ribbons in the framework. Alumination of sepiolite not only created a cation exchange capacity useful for redox centers dispersion without loss of crystallinity, but it altered fundamentally the catalytic properties of the sepiolite support itself. Being more acidic, the activity for ethanol dehydration was increased threefold at 400°C to 85%. Upon dispersion of vanadyl cations, the conversion of ethanol was further increased. A detailed catalytic study of the acetaldehyde as a cofeed is currently in progress.

At a more fundamental level, the possibility to apply successfully secondary isomorphic substitution techniques to natural minerals was clearly established. It was shown to alter their surface properties markedly, as evidenced here on sepiolite from both spectroscopic and reactivity studies. Hopefully, this should open new vistas in the fields of chemistry where natural minerals are, or were, in extensive use such as catalysis, separation science, colloid science, and surface chemistry.

ACKNOWLEDGMENTS

This work was supported by DOE Grant DE-FG02-90 ER 1430. NSF Grant DIR-8719808 and NIH Grant RR 04095, which have partly supported the purchase of the GN 500 NMR instrument, are also gratefully acknowledged. One of us J.-B. d'E. expresses his gratitude to the UWM Graduate School for a dissertation fellowship. D. Coster must be thanked for helping with transatlantic communications, Dr. O. Clause of the Institut Français du Pétrole for very critically reviewing this manuscript, and Professor Legrand for providing time for its revision at the ESPCI.

REFERENCES

1. van Bekkum, H., Flanigen, E. M., and Jansen, J. C., Eds., "Introduction to Zeolite Science and Practice." Elsevier, Amsterdam, 1991.
2. Espinose de la Caillerie, J.-B. d', and Fripiat, J. J., *Clays Clay Miner.* **39,** 270 (1991).
3. Espinose de la Caillerie, J.-B. d', and Fripiat, J. J., *Catal. Today* **14,** 125 (1992).
4. This investigation is part of a PhD thesis in which extensive literature review as well as experimental details can be found: Espinose de la Caillerie, J.-B. d', Ph.D. Thesis, University of Wisconsin-Milwaukee, 1992. Available from UMI Dissertation Services: Ann Arbor, Michigan, cat. no. 9317620.
5. Guggenheim, S., and Eggleton, R. A., *in* "Hydrous Phyllosilicates (Exclusive of Micas)" (S. W. Bailey, Ed.), Review in Mineralogy, Vol. 19, p. 683. Mineralogical Society of America, Washington DC, 1988.
6. Inagaki, S., Fukushima, Y., Doi, H., and Kamigaito, O., *Clay Miner.* **25,** 99 (1990).
7. Preisinger, A., *Clays Clay Miner., Proc. Conf.* **10,** 365 (1963).
8. Serna, C., Ahlrichs, J. L., and Serratosa, J. M., *Clays Clay Miner.* **23,** 452 (1975).
9. Ruiz-Hitzky, E., and Casal, B., *J. Catal.* **92,** 291 (1985).
10. Campelo, J. M., Garcia, A., Luna, S., and Marinas, J. M., *Clay Miner.* **22,** 233 (1987).
11. Dandy, A. J., and Nadiye-Tabbiruka, M. S., *Clays Clay Miner.* **30,** 347 (1982).
12. Kitayama, Y., and Michishita, A., *J. Chem. Soc., Chem. Commun.* **9,** 401 (1981).
13. Kitayama, T., and Wada, T., Japan Kokai 57:169429, 1981. [in Japanese]
14. Kitayama, A., Hoshina, T., Kimura, T., and Asakawa, T., *in* "Proceedings, 8th International Congress on Catalysis, Berlin, 1984, Vol. 5, p. 647. Dechema, Frankfurt-am-Main, 1984.
15. Corma, A., Misfud, A., and Pérez Pariente, J., *Ind. Eng. Chem. Res.* **27,** 2044 (1988). See also patent references therein.
16. Aramendía, M. A., Borau, V., Jiménez, C., and Marinas, J. M., *Appl. Catal.* **10,** 347 (1984).
17. Aramendía, M. A., Borau, V., Jiménez, C., Marinas, J. M., and Sempere, M. E., *Can. J. Chem.* **65,** 2791 (1987).
18. Aramendía, M. A., Borau, V., Jiménez, C., Marinas, J. M., Sempere, M. E., and Urbano, F. J., *Can. J. Chem.* **70,** 74 (1992).
19. Laperche, V., Lambert, J. F., Prost, R., and Fripiat, J. J., *J. Phys. Chem.* **94,** 8821 (1990).
20. Pinnavaia, T. J., *Science* **220,** 365 (1983).
21. Imai, N., Otsuka, R., Nakamura, T., and Koga, M., *Bull. Sci. Eng. Res. Lab., Waseda Univ.* **46,** 11 (1969).
22. Fahey, J. F., Ross, M., and Axelrod, J. M., *Am. Mineral.* **46,** 270 (1960).
23. Corma, A. C., Mifsud, A. C., and Perez, J. P., U. S. Patent 4,542,002 (1985).
24. Corma, A., Pérez-Pariente, J., and Soria, J., *Clay Miner.* **20,** 467 (1985).
25. Mifsud, A., Corma, A., and García, I., *Mater. Lett.* **6,** 436 (1988).
26. Corma, A., and Martín-Aranda, R. M., *J. Catal.*, **130,** 130 (1991).
27. Pérez Pariente, J., Fornés, V., Corma, A., and Mifsud, A., *Appl. Clay Sci.* **3,** 299 (1988).
28. Corma, A., Perez-Pariente, J., Fornes, V., and Mifsud, A., *Clay Miner.* **19,** 673 (1984).
29. Corma, A., and Perez-Pariente, J., *Clay Miner.* **22,** 423 (1987).
30. Sun, A., M. Sc. Thesis, University of Wisconsin–Milwaukee, 1994.
31. Alvarez, A., Aragon, J. J., and Perez-Castells, R., European Patent 0170299 (1984).
32. Baes, C. F., and Mesmer, R. E., "The Hydrolysis of Cations." Wiley, New York, 1976.
33. Bain, D. C., and Smith, B. F., *in* "A Handbook of Determinative Methods in Clay Mineralogy" (M. J. Wilson, Ed.), p. 258. Chapman and Hall, New York, 1987.
34. Vega, S., *J. Chem. Phys.* **68,** 5518 (1978).
35. Espinose de la Caillerie, J.-B. d', and Fripiat, J. J., *Clay Miner.* **29,** 313 (1994).
36. Gregg, S. J., and Sing, K. S. W., "Adsorption, Surface Area and Porosity," 2nd ed. Academic Press, London, 1982.
37. Parry, E. P., *J. Catal.* **2,** 371 (1963).
38. Centi, G., Pinelli, D., and Trifirò, F., *J. Mol. Catal.* **59,** 221 (1990).
39. Centi, G, Perathoner, S., Trifirò, F., Aboukais, A., Aissi, C. F., and Guelton, M., *J. Phys. Chem.* **96,** 2617 (1992).
40. Martini, G., Ottaviani, M. F., and Seravalli, G. L., *J. Phys. Chem.* **79,** 1716 (1975).
41. Campbell, R. F., and Freed, J. H., *J. Phys. Chem.* **84,** 2668 (1980).
42. McBride, M. B., *Clays Clay Miner.* **27,** 91 (1979).
43. Oldfield, E., Kinsey, R. A., Montez, B., Ray, T., and Smith, K. A., *J. Chem. Soc., Chem. Commun.*, 254 (1982).
44. Eckert, H., and Wachs, I. E., *J. Phys. Chem.* **93,** 6796 (1989).
45. Lapina, O. B., Matikhin, V. M., Nosov, A. V., Beutel, T., and Knözinger, H., *Catal. Lett.* **13,** 203 (1992).
46. Das, N., Eckert, H., Hu, H., Wachs, I. E., Walzer, J. F., and Feher, F. J., *J. Phys. Chem.* **97,** 8240 (1993).
47. de las Pozas, C., Lopez-Cordero, R., Gonzalez-Morales, J. A., Travieso, N., and Roque-Malherbe, R., *J. Mol. Catal.* **83,** 145 (1993); and references therein.
48. Centi, G., Tvarůžková, Z., Trifirò, F., Jírů, P., and Kubelková, L., *Appl. Catal.* **13,** 69 (1984).
49. Cavani, F., Trifirò, F., Jírů, P., Habersberger, K., and Tvarůžková, Z., *Zeolites* **8,** 12 (1988).
50. Sass, C. E., Chen, X., and Kevan, L., *J. Chem. Soc., Faraday Trans.* **86,** 189 (1990).
51. Inomata, M., Mori, K., Miyamoto, A., and Murakami, Y., *J. Phys. Chem.* **87,** 761 (1983).
52. Che, M., Canosa, B., and Gonzalez-Elipe, A. R., *J. Phys. Chem.* **90,** 618 (1986).
53. Occelli, M. L., Maxwell, R. S., and Eckert, H., *J. Catal.* **137,** 36 (1992).
54. Clark, G. M., and Morley, R., *J. Solid State Chem.* **16,** 429 (1976).
55. Arundale, E., and Mikeska, L. A., *Chem. Rev.* **51,** 505 (1952).
56. Yamaguchi, T., Nishimichi, C., and Kubota, A., *Prepr.—Am. Chem. Soc., Div. Pet. Chem.* **36,** 640 (1991).